



Crustal deformation and source models of the Yellowstone volcanic field from geodetic data

D. W. Vasco,¹ C. M. Puskas,² R. B. Smith,² and C. M. Meertens³

Received 20 July 2006; revised 10 February 2007; accepted 28 March 2007; published 6 July 2007.

[1] Geodetic observations, comprising Interferometric Synthetic Aperture Radar (InSAR), Global Positioning System (GPS), and precision leveling measurements, are used to infer volume change in the subsurface associated with the dynamics of the Yellowstone volcanic system. We focus primarily on the Yellowstone Caldera and its related magmatic, hydrothermal, and fault systems. It appears that known faults play a significant role in controlling crustal volume increases and decreases due to the migration of volcanic and hydrothermal fluids. For example, over 5 cm of subsidence from 1992 to 1995 is associated with source volume changes 6–10 km beneath the NW-trending Elephant Back fault zone and a north-trending fault cutting across the caldera. Furthermore, we are able to image an episode of fluid intrusion near the northern edge of the caldera. The intrusion is elongated in the north-south direction and is parallel to the north-trending volume decrease. The primary intrusion and related hydrothermal activity occurred between 1996 and 2000, though the volume changes appear to have continued, shallowed, and changed shape between 2000 and 2002. There is evidence that the intrusive activity influenced extensional faults to the north of the caldera.

Citation: Vasco, D. W., C. M. Puskas, R. B. Smith, and C. M. Meertens (2007), Crustal deformation and source models of the Yellowstone volcanic field from geodetic data, *J. Geophys. Res.*, 112, B07402, doi:10.1029/2006JB004641.

1. Introduction

1.1. Background

[2] The Yellowstone volcanic field is the youngest in a series of progressively older silicic volcanic centers, extending 800 km NE along the Snake River Plain in the western US. The Yellowstone volcanic field is energetic, with measured thermal fluxes averaging 1500–2000 mW m⁻², over thirty times higher than the continental average, and contains the world's largest concentration of geysers, hot springs, and fumaroles. The terrain and local geologic structure were shaped by three explosive caldera-forming silicic eruptions at 2 Ma, 1.3 Ma, and 634,000 years ago. The youngest caldera eruption created a 45-km-wide by 75-km-long caldera, termed the Yellowstone Caldera (Figure 1). The formation of the caldera was followed by magmatic resurgence, as evidenced by two structural domes and two lines of N- to NW-trending volcanic vents (Figure 1). The volcanic vents have fed over 30 post-collapse ash and rhyolite flows. The youngest of these events was 70,000 years ago. *P* wave tomographic imaging has revealed a low-velocity crustal body underlying the entire Yellowstone Caldera from 8 to 16 km in depth. The low-velocity body is thought to represent a hot, crystallizing

magma system composed of partial melts and related fluids and gases [Husen and Smith, 2004].

[3] The Yellowstone volcanic system is located in a tectonically active zone of extension at the eastern edge of the Basin and Range Province. The caldera is also the vertex of multiple north- to northwest-trending normal faults. The extent to which the faults interact with and control the magmatic and hydrothermal system is not currently known. However, modeling suggests that fault-induced stress interaction with the 1959 Hebgen Lake earthquake (*M*7.5) triggered extended aftershocks across the western Yellowstone Caldera [Chang and Smith, 2002]. Viscoelastic relaxation from the Hebgen Lake event continues to add a N-S extension of a few mm/year at the NW edge of the caldera and adjacent areas (W. L. Chang and R. B. Smith, Lithospheric rheology from postseismic deformation of a *M* = 7.5 normal-faulting earthquake with implications for continental kinematics, submitted to *Journal of Geophysical Research*, 2006). On the basis of their modeling results, viscoelastic processes are estimated to contribute up to ~1 mm/year N-S extension within the caldera. Because the modeled viscoelastic effects are small for the time periods studied, we shall not correct for the deformation associated with the Hebgen Lake earthquake relaxation.

1.2. Geodetic Monitoring

[4] Through an extensive monitoring effort, it has become clear that the Earth's surface above the Yellowstone Caldera is in an almost constant state of unrest. Initial measurements from precision leveling of benchmarks, established in 1923, revealed uplift of ~1 m within the

¹Berkeley Laboratory, University of California, Berkeley, California, USA.

²Department of Geology and Geophysics, University of Utah, Salt Lake City, Utah, USA.

³University NAVSTAR Consortium, Boulder, Colorado, USA.

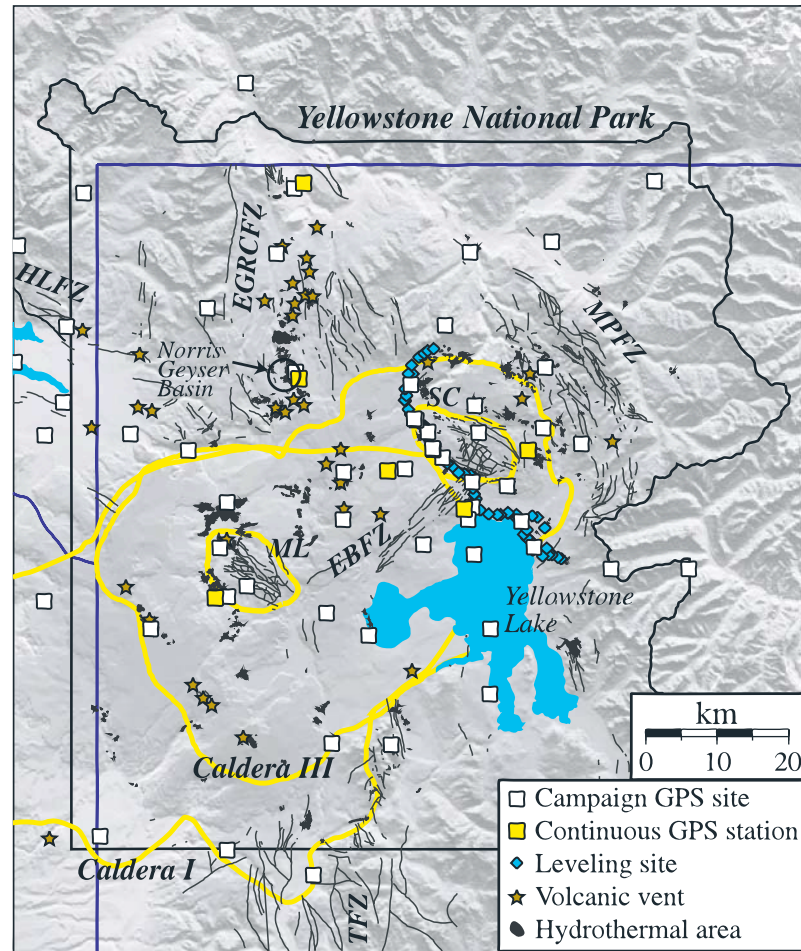


Figure 1. Index map of the Yellowstone Plateau showing geodetic stations, calderas, resurgent domes, hydrothermal areas, and faults. Caldera III = 0.64 Ma caldera, Caldera I = 2.1 Ma caldera, SC = Sour Creek resurgent dome, ML = Mallard Lake resurgent dome, MPFZ = Mirror Plateau fault zone, EBFZ = Elephant Back fault zone, EGRC = East Gallatin-Reese Creek fault zone (aka Norris-Mammoth corridor). Note that Caldera II is nested at the western boundary of Caldera I and is outside the map area.

caldera between 1923 and 1985 [Pelton and Smith, 1979, 1982; Dzurisin and Yamashita, 1987]. Smith and Meertens [1989] and Dzurisin *et al.* [1990] found variations in the rate of uplift for the northeast and southwest portions of the caldera through 1984. The uplift subsequently abated, giving way to subsidence of over 12 cm by 1990 [Dzurisin *et al.*, 1990]. This reversal was confirmed by three-component Global Positioning System (GPS) observations [Meertens and Smith, 1991]. Satellite radar interferometry [Interferometric Synthetic Aperture Radar (InSAR)], which measures changes in distance between an orbiting satellite and the Earth's surface [Massonnet and Feigl, 1998], together with the GPS observations, have shown how truly dynamic the Yellowstone Caldera is [Wicks *et al.*, 1998; Dzurisin *et al.*, 1999]. At Yellowstone, surface deformation was found to be highly variable, both in space and in time, with significant changes from year to year and with deformation appearing to migrate across the caldera.

[5] Recent geodetic evidence suggests that the subsidence of the early 1990s reverted to uplift of about 1.5 cm/year around 1995 [Wicks *et al.*, 1998; Dzurisin *et al.*, 1999; Puskas *et al.*, 1998] (Figure 2). The uplift is concentrated at

the northern edge of the caldera. Net subsidence of 2.0 cm/year was again observed within the caldera between 2000 and 2001 and between 2001 and 2002 [Wicks *et al.*, 2006]. These dramatic changes are corroborated by an extensive array of GPS and leveling measurements [Meertens *et al.*, 2000] (Figure 3). The InSAR and GPS data sets are found to be in both qualitative and quantitative agreement (Figure 4). GPS and InSAR data are complementary data sets, each important in its own regard. GPS observations provide estimates of the horizontal components of displacement which are helpful in constraining the geometry of subsurface volume change [Dieterich and Decker, 1975]. InSAR data provide dense spatial sampling of the projection of the displacement components onto the vector pointing from the sample points on the Earth's surface to the satellite.

[6] The Holocene geologic record, as preserved in uplifted terraces of Yellowstone Lake, supports these historic and present-day observations of cycles of uplift and subsidence [Locke and Meyer, 1994]. Precise spirit leveling [Reilinger *et al.*, 1977] and trilateration measurements [Savage *et al.*, 1993] have revealed deformation to the north and west of Yellowstone Caldera, primarily caused

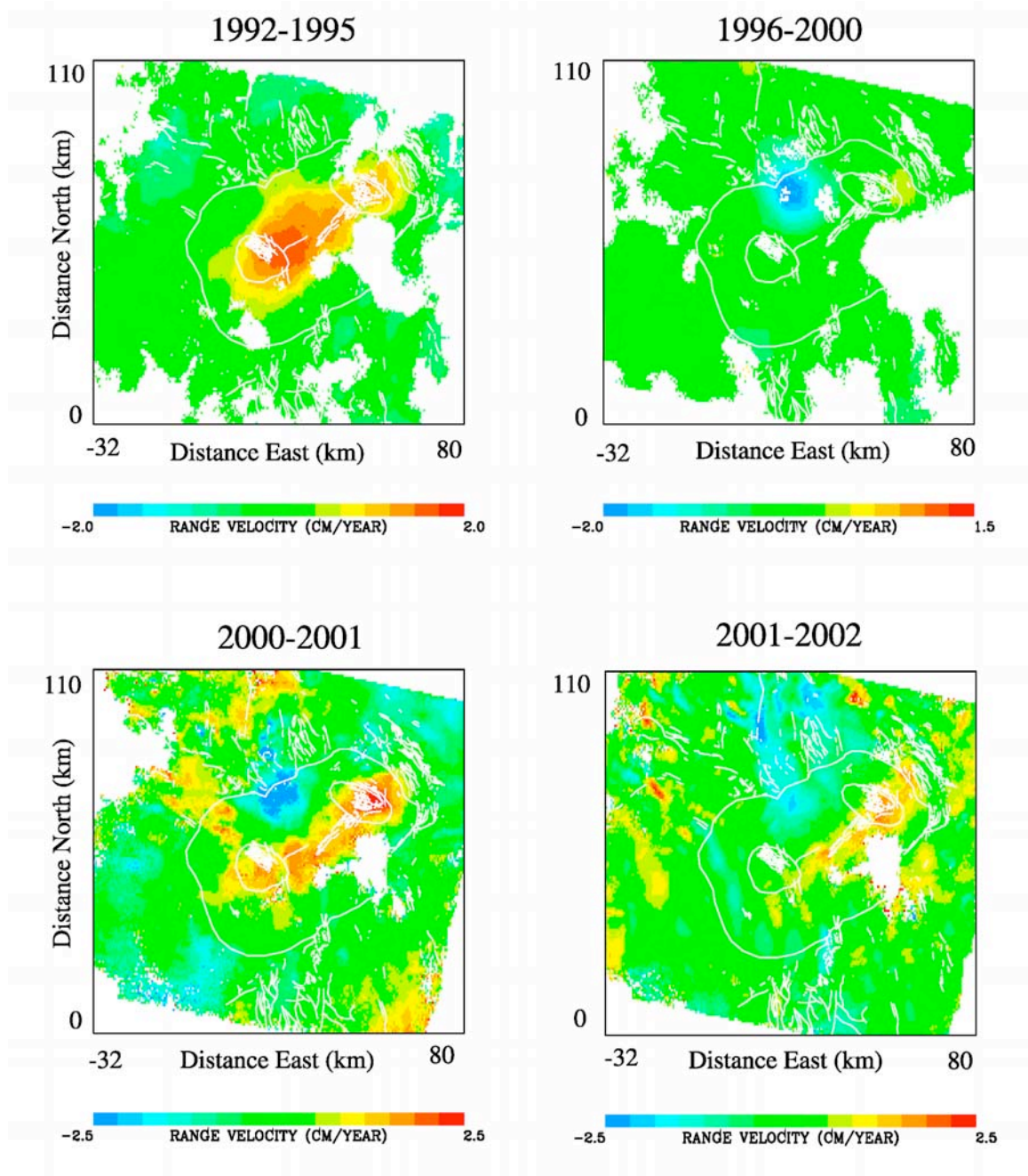


Figure 2. Range velocity, the rate at which points on the Earth are moving toward or away from a remote observation point, as calculated from Interferometric Synthetic Aperture Radar (InSAR) measurements. Negative values indicate decreasing distance over time (uplift), while positive values signify increasing distance (subsidence). White regions denote the absence of range velocity estimates. The outline of the Yellowstone Caldera and mapped faults are indicated by white lines.

by the Hebgen Lake earthquake. Paleoseismic studies of the Teton fault, to the south of the caldera, extrapolate regional extension rates of 0.1 to 0.2 mm/year [Byrd *et al.*, 1994].

1.3. Source Modeling

[7] In order to gain insight into the factors controlling surface deformation, we construct very general models of subsurface volume change that are compatible with the observed InSAR, GPS, and leveling data from the various

time intervals shown in Figure 2. Our approach, based upon the inversion of the multiple types of geodetic data, is exploratory in nature. That is, rather than prescribe a specific geometric configuration, such as a point source, we allow for an arbitrary, three-dimensional distribution of subsurface volume change [Vasco *et al.*, 2002a]. The resulting pattern of subsurface volume change and source geometry provides insight into the factors controlling observed surface deformation. With an improved under-

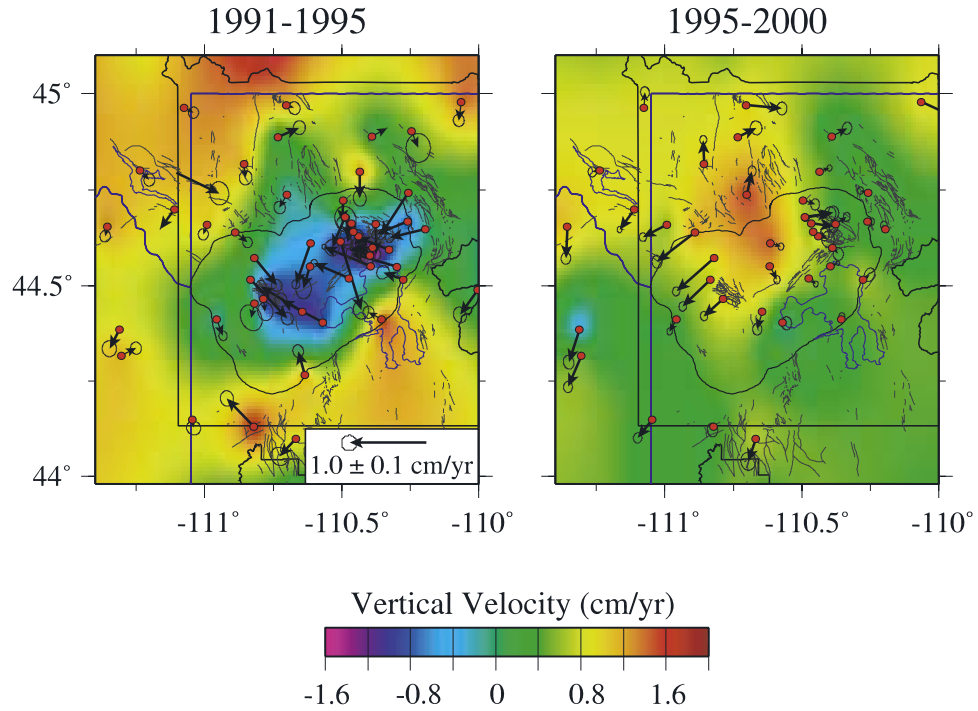


Figure 3. Point velocity estimates obtained from Global Positioning System (GPS) satellite observations [Meertens and Smith, 1991; Puskas et al., 1998]. The arrows indicate horizontal velocity vectors, while the color scale indicates the rate of vertical displacement. The outline of the caldera and the two resurgent domes are indicated by solid black lines. The ellipses plotted at the end of the displacement vectors signify an error of one sigma.

standing of the nature of the controlling features, one may then go on to construct more detailed and prescribed models for the sources of deformation, particularly magmatic and hydrothermal sources and the time migration of resulting fluids.

[8] We feel that such an exploratory approach is warranted at this stage because of the heterogeneity of material properties in the Yellowstone region. Because of the presence of layering and faults, the Earth is certainly not homogeneous, and modeling based upon a homogeneous

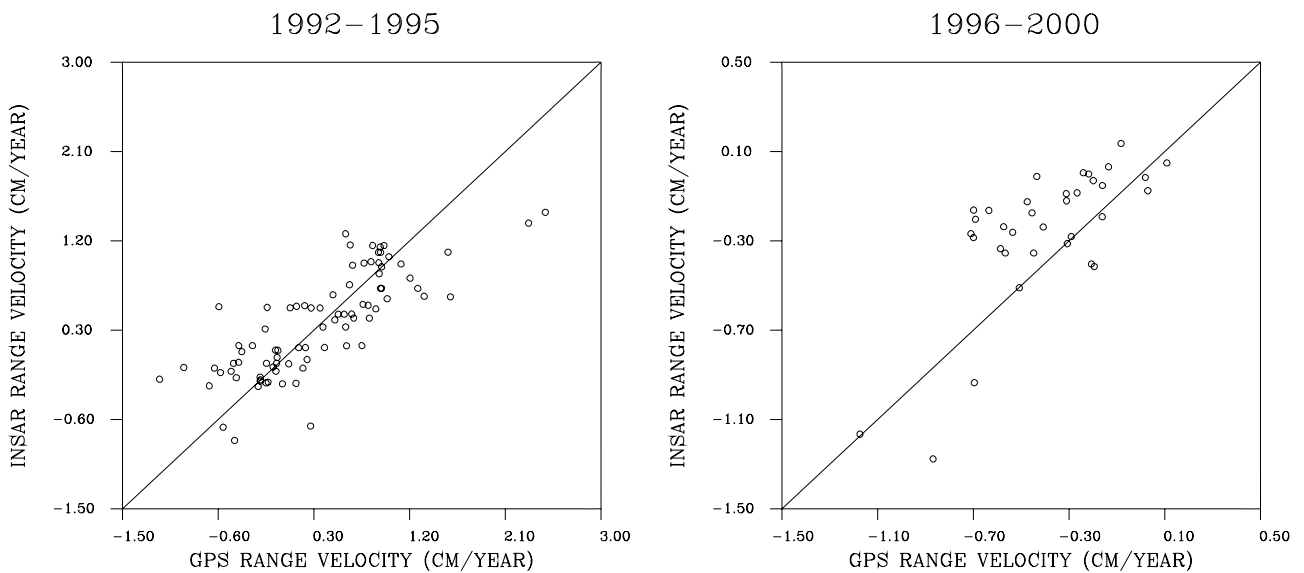


Figure 4. A comparison between range velocity predicted using GPS displacement data and observed range velocity associated with the InSAR pixel nearest to the GPS station. The GPS displacement components were projected onto the satellite look vector to produce a range change estimate. Because the time intervals for the InSAR and GPS do not coincide, the values were converted to velocities. Thus some of the scatter may be due to deformation in the nonoverlapping time boundaries.

half-space, as done here and in most studies, is certainly an idealization. It has been shown that if zones of low rigidity are present in the Earth, they may amplify the displacement field at the surface [Chinnery and Jovanovich, 1972]. However, studies in complex volcanic regions, such as the Long Valley caldera, have found that factors such as layering do not significantly impact the modeling of uplift because of volume change within the Earth [Battaglia and Segall, 2004]. Another source of heterogeneity in the material properties are strong lateral and vertical variations in temperature in volcanic regions [Newman et al., 2001; Newman et al., 2006]. Such temperature-induced variations are difficult to model because they require prior knowledge of the distribution of volcanic bodies at depth. However, it is known from the distribution of earthquakes, gravity, and magnetic anomalies that the major induced thermal variations are relatively uniform across the Yellowstone Caldera [Smith and Braile, 1994]. Thus it should be acceptable to model the region within the Yellowstone Caldera as a laterally uniform structure. At the boundaries of the caldera, the gradient in material properties may be significant, and some care must be given to interpretations near the edge of the caldera.

[9] We feel that, while a quantitative interpretation of surface deformation may not be reliable at this stage, an exploratory approach is certainly useful. For example, the locations and general features of the volume change anomalies are probably robust. While variations in rhyology might change the shape of an anomaly slightly, it is unlikely that they would result in a significant lateral mislocation of inferred volume change. However, the same robustness cannot be claimed for depth estimates. Depth resolution is poor in general, and errors in rheology could possibly produce significant depth variations. For this reason, we do not place great emphasis on the depth of the features, focusing instead on their location and shape.

2. Methodology

[10] In this section, we describe the approach we use to infer subsurface volume change associated with the Yellowstone volcanic system. The methodology is a refinement and extension of earlier approaches for estimating volume change from geodetic data [Vasco et al., 1988; Vasco et al., 1990; Vasco et al., 2002a, 2002b]. As mentioned in section 1, the technique is exploratory in nature, as we allow for an arbitrary three-dimensional source. We do this in order to better understand the geologic structures controlling subsurface fluid flow. Before describing the inversion methodology, we present the technique used to relate surface deformation to volume change in the subsurface. Because the method is described elsewhere, only a brief overview is given. In our final interpretation at the end of the paper, we integrate our geodetic models with seismic tomographic images of crustal magmatic-hydrothermal bodies, providing an independent validation of our models.

2.1. Surface Deformation Due to Volume Change Within the Earth: The Forward Problem

[11] We model the source of the Earth's surface deformation as internal volume change. That is, we assume that the movement of material, typically fluids and gases generated

by hydrothermal and magmatic activity, induces deformation of the Earth's surface. Note that some internal strain, such as slip on a fault, will not be interpreted correctly. However, in a active hydrothermal-magmatic system, as at the Yellowstone Caldera, a volumetric source component is a reasonable assumption. We should point out that volume changes do not occur in isolation. Stated another way, volume or mass is not simply created within the Earth. Rather, a volume increase beneath the Earth's surface must be due to the movement of material or energy from within. The uplift and radial expansion due to intrusion will be accompanied by subsidence radial contraction due to migration of material from a source region. Typically, the source region is deep enough that the surface deformation associated with the volume decrease is small, well within the noise of the observations.

[12] The first task is to relate the subsurface volume change to the displacement of the Earth's surface. The basic idea is that, for an Earth which deforms elastically, there is a linear relationship between a fractional volume change at a point \mathbf{y} , $\Delta v(\mathbf{y})$ within a source volume V , and the l th component of surface displacement. The mathematical representation of such a relationship is termed a Green's function [Stakgold, 1979]

$$u_l(\mathbf{x}) = \int_V G_l(\mathbf{x}, \mathbf{y}) \Delta v(\mathbf{y}) d\mathbf{y} \quad (1)$$

[Aki and Richards, 1980]. Fractional volume change is the ratio of the volume change to the volume under consideration, V_0 , for example, $\Delta v = (V - V_0)/V_0$ where V_0 is the original volume and V is the new volume. The quantity $G_l(\mathbf{x}, \mathbf{y})$, the Green's function [Roach, 1970; Stakgold, 1979], is a function of the observation point \mathbf{x} and the source point \mathbf{y} . The nature and complexity of the Green's function depends upon the assumed medium and the physical model. We shall assume that the source lies within a homogeneous elastic half-space so that the Green's function is given by

$$G_l(\mathbf{x}, \mathbf{y}) = \frac{(\nu + 1)}{3\pi} \frac{(x_l - y_l)}{S^3} \quad (2)$$

where ν is Poisson's ratio and

$$S = \sqrt{(x_1 - y_1)^2 + (x_2 - y_2)^2 + (x_3 - y_3)^2} \quad (3)$$

is the distance between the source point \mathbf{y} and the observation point \mathbf{x} [Maruyama, 1964; Okada, 1985; Vasco et al., 1988].

[13] The expression for displacement given above is sufficient for modeling leveling ($l = 3$) and GPS ($l = 1, 2, 3$) observations but must be modified in order to treat InSAR range changes. Range is the distance from a fixed point in space to the point of interest on the surface of the Earth [Massonnet and Feigl, 1998]. Synthetic Aperture Radar (SAR) imagery is generated by an orbiting satellite which backscatters radar waves from the surface of the Earth [Massonnet and Feigl, 1998]. InSAR is an interferometric technique in which the phase shift between successive complex traces of backscattered energy is calculated for

each pixel of the SAR image [Zebker *et al.*, 1994]. The phase shift ϕ is linearly related to the range change $\delta\rho$ and a topographic contribution [Zebker *et al.*, 1994; Bürgmann *et al.*, 2000]. Using this relationship, one can solve for range change. Using a digital terrain model (DTM) one can obtain a precision of 0.25–1.25 cm [Gabriel *et al.*, 1989]. Using multiple satellite passes, it is possible to solve for biases, such as topography, directly rather than simply correcting them, allowing one to estimate the range change to a precision of a few millimeters [Zebker *et al.*, 1994]. The basic datum in InSAR is the range change $\delta\rho$ over some interval of time. If the surface of the Earth deforms during this period, the accumulated displacements of the reflection point are projected onto the range vector, \mathbf{l} , a unit vector which points toward the satellite. Thus,

$$\delta\rho(\mathbf{x}) = u_l \cdot l_l \quad (4)$$

where we invoke the convention of summing over repeated indices. From equation (1), we find that

$$\delta\rho(\mathbf{x}) = \int_V R(\mathbf{x}, \mathbf{y}) \Delta v(\mathbf{y}) d\mathbf{y} \quad (5)$$

where

$$R(\mathbf{x}, \mathbf{y}) = l_l \cdot G_l(\mathbf{x}, \mathbf{y}) \quad (6)$$

is the projection of the displacement Green's functions onto the range vector. The components of the vector \mathbf{l} are known from the geometry of the satellite's orbit. Note that, if different orbital geometries are available, it is possible to acquire different combinations of displacement components. Normalizing by the time interval, we can present the results in terms of range velocity. Using range velocity makes it easier to compare changes over time intervals of varying lengths.

2.2. Geodetic Imaging of Subsurface Volume Change: The Inverse Problem

[14] In this subsection, we outline a technique for mapping observed surface displacement into subsurface volume change. The methodology is an adaptation of an approach used in an earlier analysis of leveling data from the Yellowstone region [Vasco *et al.*, 1990], the nonnegative least squares algorithm of Lawson and Hanson [1974]. The constraint equations are provided by the linear equations (1) and (5), which relate volume change within the Earth $\Delta v(\mathbf{y})$ to surface displacements $u_l(\mathbf{x})$ and range change $\delta\rho(\mathbf{x})$ [Vasco *et al.*, 2002a]. Equation (1) is appropriate for leveling and GPS data, while equation (5) is used for InSAR observations. Given a set of M measurements, there will be a set of linear constraint equations which we write in vector-matrix form

$$\mathbf{u} = \mathbf{G}\mathbf{v} \quad (7)$$

where \mathbf{u} is a vector containing the various components of $u_l(\mathbf{x})$ as well as the range-change data, $\delta\rho$, recorded at the observation points. Note that, through the inclusion of InSAR range-change measurements, the data can number in

the tens of thousands. As discussed in Vasco *et al.* [1988, 1990, 2002a], the unknown vector \mathbf{v} represents the effective subsurface volume changes. In particular, we subdivide a region of the subsurface into a grid of cells, each of which may undergo a distinct fractional volume change. We solve equation (7) for the fractional volume change within each grid block.

[15] Because the equations may be redundant, the system of equation (7) may be nearly singular, and the solution may be unstable with respect to errors in the observations and the coefficient matrix \mathbf{G} . This is particularly true when there are multiple layers in our grid of cells. The fractional volume change for cells in the lower layers of such a grid tend to be poorly resolved by geodetic data [Vasco *et al.*, 2002a, 2002b]. In order to stabilize the system, we add equations which penalize rough models and models with fractional volume changes which deviate significantly from a preferred volume change model \mathbf{v}_0 , as described in Vasco *et al.* [2002a]. In terms of a least squares approach, we define a penalized misfit function

$$P(\mathbf{v}) = \|\mathbf{u} - \mathbf{G}\mathbf{v}\|^2 + W_r \|\mathbf{D}\mathbf{v}\|^2 + W_n \|\mathbf{v} - \mathbf{v}_0\|^2 \quad (8)$$

where \mathbf{D} is a matrix approximation to an operator which computes the spatial derivative of the volume change, \mathbf{v}_0 is a preferred volume change model, and $\|\mathbf{v}\|$ denotes the magnitude of the vector \mathbf{v} . The scalars W_r and W_n are weights for the roughness and norm penalty terms, controlling the size of these terms with respect to the data-fitting term. The terms in the penalized misfit function $P(\mathbf{v})$ can be combined into a composite function

$$P(\mathbf{v}) = \|\mathbf{E}\mathbf{v} - \mathbf{f}\|^2 \quad (9)$$

where

$$\mathbf{E} = \begin{pmatrix} \mathbf{G} \\ \sqrt{W_r}\mathbf{D} \\ \sqrt{W_n}\mathbf{I} \end{pmatrix} \quad (10)$$

and

$$\mathbf{f} = \begin{pmatrix} \mathbf{u} \\ \mathbf{0} \\ \sqrt{W_n}\mathbf{v}_0 \end{pmatrix} \quad (11)$$

[16] In addition to the penalty terms, we also use inequality constraints to reduce the nonuniqueness associated with the inverse problem [Sabatier, 1977]. The inequality constraints are motivated by the fact that for an intrusion, all of the volume change will be positive. Similarly, for a source region where there is net loss of material, the volume changes will be negative. Thus for time intervals in which subsidence or uplift dominate, such as 1992–1995 and 1996–2000 in Figure 2, we require that the volume change be negative or positive, respectively. For time intervals in which both uplift and subsidence are observed, 2000–2001 and 2001–2002 in Figure 2, we could require that volume change in a particular region is of one sign, either all positive or all negative, while volume change in another

region is of the opposite sign. In assigning a particular sign to the volume change, we are making specific assumptions. For example, by only allowing for volume increase in the time interval 1996–2000, we are only modeling the intrusion and ignoring volume decreases associated with the deeper source of the intruding volume. By including inequality constraints, we are eliminating trade-offs between positive and negative volume change which can lead to additional nonuniqueness in the inverse problem [Sabatier, 1977]. The resulting inverse problem is equivalent to minimizing

$$P(\mathbf{v}) = \|\mathbf{E}\mathbf{v} - \mathbf{f}\|^2 \quad (12)$$

subject to the inequality constraints

$$\mathbf{\Sigma}\mathbf{v} \geq \mathbf{0} \quad (13)$$

where $\mathbf{\Sigma}$ is a diagonal matrix with ± 1 on the diagonal, where the sign depends on the type of inequality associated with the grid block. The constrained optimization problem is solved using a variant of the Nonnegative Least Squares algorithm (NNLS) of Lawson and Hanson [1974]. As an aside, we also mention the conjugate gradient algorithm presented by Hestenes [1980] for the situation in which the components are nonnegative. This algorithm provides an alternative approach for solving the inverse problem in the presence of inequality constraints. An approach based upon a conjugate gradient algorithm may have some advantages in the situation in which \mathbf{E} is large and sparse.

[17] Because of the presence of inequality constraints, the inverse problem is no longer strictly linear. This complicates the estimation of uncertainties associated with our computed volume changes. We are forced to adopt a stochastic, or Monte Carlo type, estimate of model parameter errors. In particular, we add noise to the data which are designed to mimic the estimated errors in the observations. We then invert the perturbed data and obtain model parameter estimates. By conducting a large number of such inversions, we can compute a mean model parameter estimate and an associated standard error.

3. Geodetic Data Analysis

[18] In this section, we use all available geodetic data to solve for very general three-dimensional models of volume change in the crust. The approach, outlined in section 2, is a regularized, nonnegative least squares algorithm which was applied to leveling data by Vasco *et al.* [1990]. We have modified the algorithm to allow for the inclusion of various data types, including GPS and InSAR observations. Thus the data sets will be much more extensive than those used by Vasco *et al.* [1990].

3.1. Observed Yellowstone Geodetic Data

[19] The basic data, shown in Figures 2 and 3, consist of InSAR data provided by Chuck Wicks of the USGS, GPS data produced by several campaigns in the Yellowstone region [Meertens and Smith, 1991; Meertens *et al.*, 2000; Puskas *et al.*, 1998; Puskas *et al.*, 2007], and precision leveling data taken along a road within Yellowstone National Park [Dzurisin *et al.*, 1994].

3.1.1. InSAR Data

[20] The InSAR data are described elsewhere [Wicks *et al.*, 1998, 2006], and these papers should be consulted for information concerning processing and data reduction. The only additional step we applied to these data involved stacking three sets of interferograms to improve the signal-to-noise ratio for the 1992 to 1995 time interval. We added two interferograms which spanned a time interval from August 1992 to June 1995 (orbits 5697 and 10206 in Wicks *et al.* [1998]). The range change was converted to range velocity (cm/year) and averaged with the velocities associated with interferograms corresponding to orbit pairs 5697–20570 and 5196–21572. The composite range velocity estimates are shown in Figure 2 in the panel labeled 1992–1995. The range changes from the other three time intervals, 1996–2000, 2000–2001, and 2001–2002 were derived from single pairs of SAR images. InSAR observations provide a large data set, constraining the range change associated with 30-m by 30-m pixels covering the Yellowstone region. In fact, each panel in Figure 2 represents over 21,000 range-change measurements. As noted above, the removal of topography using a digital terrain model results in an estimate of range change which is accurate to 0.25–1.25 cm [Gabriel *et al.*, 1989; Zebker *et al.*, 1994]. Another source of error is due to atmospheric disturbances which introduce noise with a standard deviation of 0.5 cm [Hoffmann *et al.*, 2003]. The combined effect of these errors is to introduce an uncertainty of approximately 1 cm for InSAR range-change estimates. Note that stacking interferograms will reduce the atmospheric noise, assuming that it is uncorrelated.

3.1.2. GPS Data

[21] The GPS data are from three of the seven field campaigns conducted by the University of Utah [Puskas *et al.*, 2007]. The surveys from 1991 to 1995 detected subsidence within the Yellowstone Caldera, which subsequently (after 1995) changed to uplift at the northern edge of the caldera, as shown in Figure 3. There are many fewer GPS observations than there are InSAR range-change data. For example, there are 84 GPS observations in the 1991–1995 panel in Figure 3. Similarly, there are just over 60 GPS measurements available in the Yellowstone region during the 1995–2000 time period. In spite of their limited number, the GPS data are valuable because they provide three components of displacement (vertical, north-south, and east-west). In fact, the horizontal velocity components are the most well resolved, with estimated errors of ± 0.02 to 0.18 cm/year. The error associated with the vertical component is much larger, ranging from ± 0.12 to 1.10 cm/year [Puskas *et al.*, 2007]. The GPS data were available for the time intervals 1991 to 1995, 1993 to 1995, and 1995 to 2000. The 1991–1995 and 1993–1995 data were linearly interpolated to estimate the changes over the interval 1992–1995. The interpolated 1992 to 1995 time period corresponds quite closely to the 1992–1995 InSAR time interval. However, the 1995 to 2000 GPS interval is longer than the InSAR interval (1996–2000). In combining the data, we scaled the GPS measurements to account for the longer time interval. Interpolation and scaling can introduce errors due to nonuniform motion within the specified time intervals. A qualitative comparison of the InSAR (Figure 2) and GPS (Figure 3) observations suggests that the pattern of defor-

mation is similar, and hence the scaling is considered to be acceptable. A plot of observed range change from InSAR data against range change predicted by nearby GPS stations (Figure 4) supports the view that the scaling does not significantly degrade the correlation between the GPS and InSAR values. The scatter for the 1996–2000 interval is not significantly greater than the scatter for the 1992–1995 interval.

3.1.3. Leveling Data

[22] The leveling data are discussed in *Dzurisin et al.* [1994] and consist of a line from Lake Butte to Canyon Junction that was surveyed annually from 1987 to 1993, and again in 1995. The leveling data were only available for the 1992 to 1995 time interval. The errors associated with the leveling measurements increases with distance along the line [*Strange*, 1981; *Pelton and Smith*, 1982; *Vasco et al.*, 1990; *Dzurisin et al.*, 1994], with a peak error of approximately 0.8 cm.

3.2. Fractional Volume Change Model

[23] In an earlier study [*Vasco et al.*, 1990], a rather crude 6×6 grid was used to infer volume changes which could give rise to uplift observed on leveling lines within the Yellowstone National Park. The block sizes associated with that grid were rather large, 11.0 km by 11.0 km by 3.0 km. Given the more extensive set of data provided by the space-based methods, InSAR and GPS, we have refined the inversion grid. Each horizontal layer of our model is decomposed into a 35×35 grid of cells. The grid blocks are 2.3 km (east-west) by 2.4 km (north-south) in lateral extent and 2.0 km thick. As noted by several investigators, the depth of the volume change trades off with the size and shape of the volume change [*Parker*, 1975; *Vasco and Johnson*, 1985]. To some degree, this trade-off is mitigated by including horizontal components in the inversion [*Dieterich and Decker*, 1975]. However, the horizontal GPS components are sparsely distributed and do not completely eliminate trade-offs that occur in depth. From previous investigations, we have found that it is possible to vary the depth boundaries of an inversion grid and still fit a set of geodetic data [*Vasco et al.*, 2002a, 2002b]. Furthermore, fractional volume change in the deeper layers of a multilayer grid tends to be poorly resolved [*Vasco et al.*, 2002a, 2002b].

[24] We use the observations concerning the resolution of fractional volume change in designing our inversion grid. Because the depth of the grid is somewhat arbitrary, we attempted to find the deepest model which is compatible with the observations. The depth boundaries are determined by increasing the depth to the top of the model until the misfit is of the order of the estimated errors. We moved the grid in 2-km increments, so possible boundaries for the top layer were 2–4 km, 4–6 km, 6–8 km, and 8–10 km. In many of our previous studies, we found that, because of the poor resolution, the inversions tended to put very little volume change below the second layer of a model [*Vasco et al.*, 2002b]. Therefore because the deeper layers tend to be poorly resolved, we chiefly used two-layer models. There was one exception, for the time interval 2001–2002, which we discuss below.

[25] The inferred subsurface volume changes are shown in Figures 5 and 6, in units of fractional volumetric strain

(change in volume per unit volume) for the four time intervals: 1992–1995, 1996–2000, 2000–2001, and 2001–2002. For ease of interpretation, we have plotted volume decreases in Figure 5 and volume increases in Figure 6. Similarly, we display the estimated errors associated with the volume decreases and increases in Figures 7 and 8, respectively. The error estimates were generated by inverting values contaminated by normally distributed random numbers. The standard errors of the random values coincide with those of the actual geodetic data. Note the increased error at the north and west edge of the modeling grid for the time intervals 1992–1995 and 1996–2000. Most likely, this is due to poor coverage in these areas, as indicated in Figure 2, coupled with the nature of the roughness regularization and the inequality constraints. In the subsections that follow, we discuss each time interval in more detail.

3.2.1. 1992–1995

[26] The InSAR and GPS data for this interval (Figures 2 and 3) indicate that the caldera subsided at a rate of more than 2 cm/year over a broad region. The GPS network within the caldera also contracted by approximately 1 cm/year during this time. Because of the lack of uplift anywhere in the region, we assume that only volume decreases are significant in the upper 10 km of the crust that we are modeling. The volume decreases may be due to a loss of pressure in a magma body induced by the movement of material or crystallization and contraction due to cooling or the transport of hydrothermal fluids from the magmatic system.

[27] In our search for the deepest model fitting the data within their errors, we find that the 1992–1995 InSAR, leveling, and GPS observations are compatible with a two-layer model with boundaries of 6–8 and 8–10 km. This finding agrees with models which contain a semisolid or plastic magma body topped by fluids and separated from the overlying brittle rock mass by a self-sealing zone of relatively impermeable material [*Fournier*, 1999]. Such a self-sealing layer is thought to underlie the region of active seismicity within the Yellowstone Caldera [*Husen and Smith*, 2004] and to lie at a depth of roughly 5 km.

[28] We conducted a joint inversion of the InSAR, GPS, and leveling data for volume change within each of the 2450 grid blocks of the model. The volume decreases within the top layer (6–8 km) of the model are shown in Figure 5. The results suggest that the surface displacements observed between 1992 and 1995 can be explained by volume decreases below the Elephant Back Fault Zone, extending from the Mallard Lake dome to beyond the Sour Creek dome. The easternmost edge of this anomaly underlies Hot Springs Basin, one of Yellowstone's largest hydrothermal systems. There is also a significant linear trend of volume decrease extending due north from the center of the caldera. This volume change is located beneath a series of volcanic vents that fed the postcollapse lava flows, indicated by the stars in Figure 5. The north-trending volume decrease follows the extension of the East Gallatin-Reese Creek fault into the caldera. Close examination of the 1992–1995 InSAR velocities in Figure 2 reveals a subtle lobe at the northern edge of the central caldera. It is this north-trending lobe that is explained by the linear volume change anomaly. The volume change in the deeper layer of the model (8–10 km) is similar in pattern but significantly diminished in

Volume Decrease

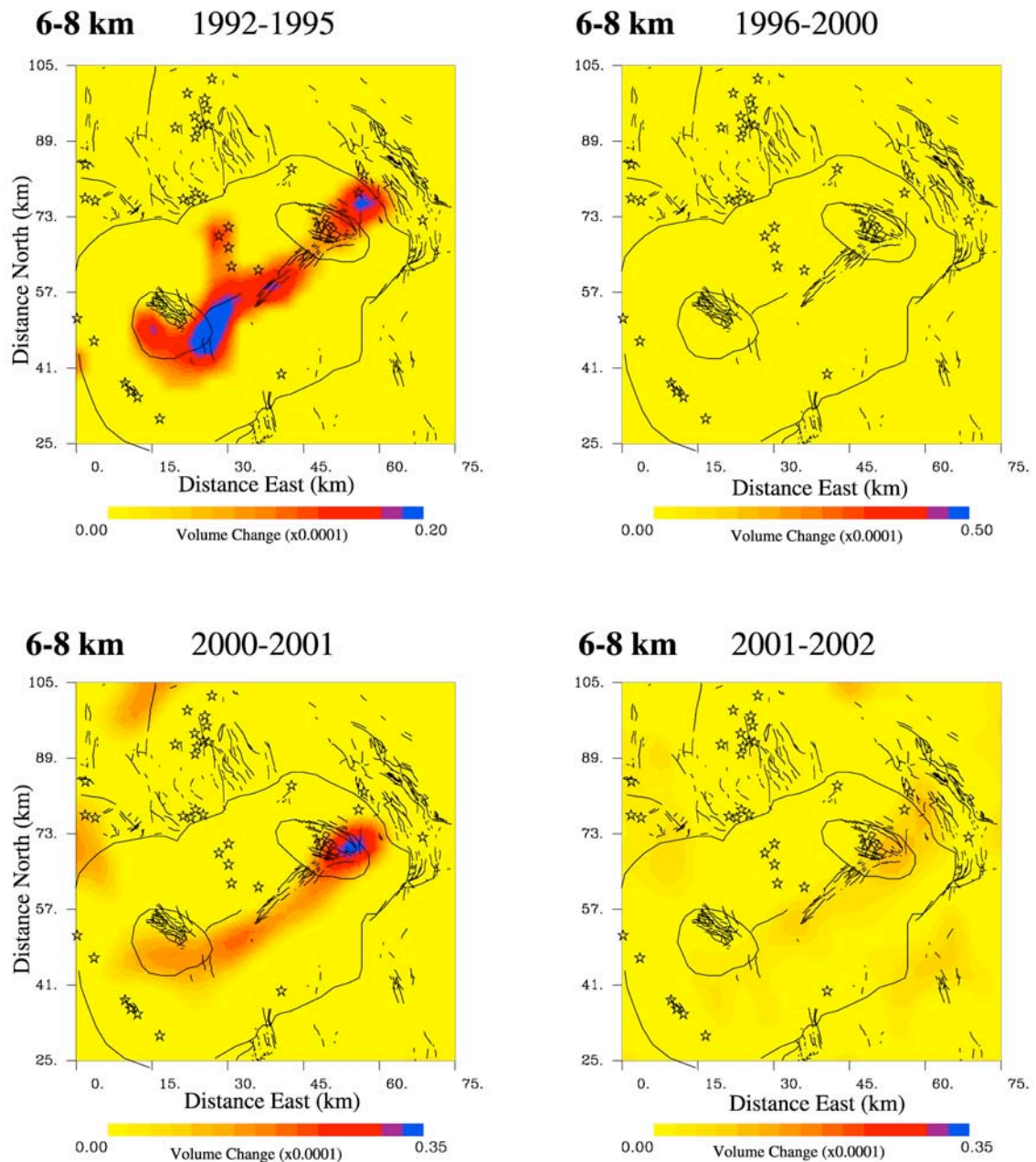


Figure 5. Estimates of subsurface volume decrease for the four time intervals. Only volume change for the uppermost layer of each model is shown. For all time intervals, the uppermost layer containing volume-significant decreases lies at 6–8 km in depth. The color scale is in terms of fractional volume change, which is unitless.

amplitude. For completeness, we have also plotted the volume increase in the topmost layer (Figure 6). Because of the negativity constraint, the volume increase is uniformly zero in the layer.

[29] Because of the negativity constraint, it is not possible to construct a formal uncertainty estimate. Rather, error estimates are generated stochastically by inverting data sets consisting of the output from a random number generator.

The random number generator output conforms to a Gaussian distribution with a variance corresponding to that of the data. A total of 100 models are generated to compute the standard error estimates (Figure 7). The error estimates may be thought of as the noise level associated with the estimates of volume decrease in Figure 5. Thus they may be used to evaluate the significance of the volume decreases within the caldera. For plotting purposes, the error estimates are also

Volume Increase

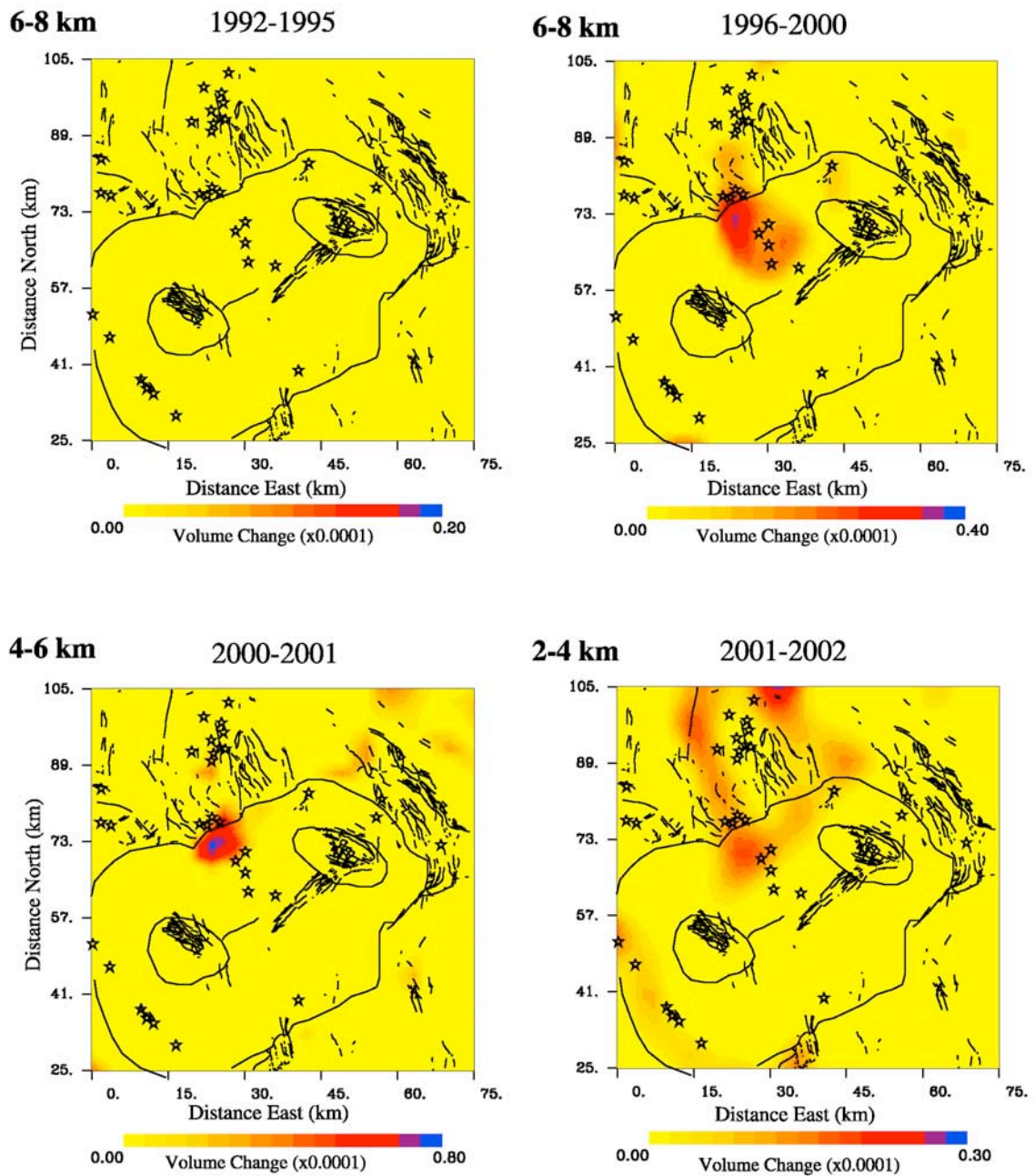


Figure 6. Estimates of subsurface volume increase for the four time intervals. Only volume change for the uppermost layer of each model is shown. For 1992–1995 and 1996–2000, the uppermost layer lies at 6–8 km in depth. For 2000–2001 and 2001–2002, the uppermost layer is 4–6 and 2–4 km in depth, respectively. The scale is in terms of fractional volume change.

shown in Figure 8, though the volume increases are constrained to be zero.

[30] The fits to the GPS, leveling, and InSAR data are shown in Figure 9. For a perfect fit, the observations would lie on the diagonal lines shown in the figures. Generally, the GPS and leveling data are fit to within their estimated standard errors (Figure 9). The larger error bars conform

to the well-known fact that the vertical GPS components are more uncertain than the horizontal components. The fit to the InSAR data is also shown in Figure 9. There is considerable scatter in the fit to the InSAR values. However, the large-scale trend of the data is matched, though the higher velocities are somewhat underpredicted.

Volume Decrease Errors

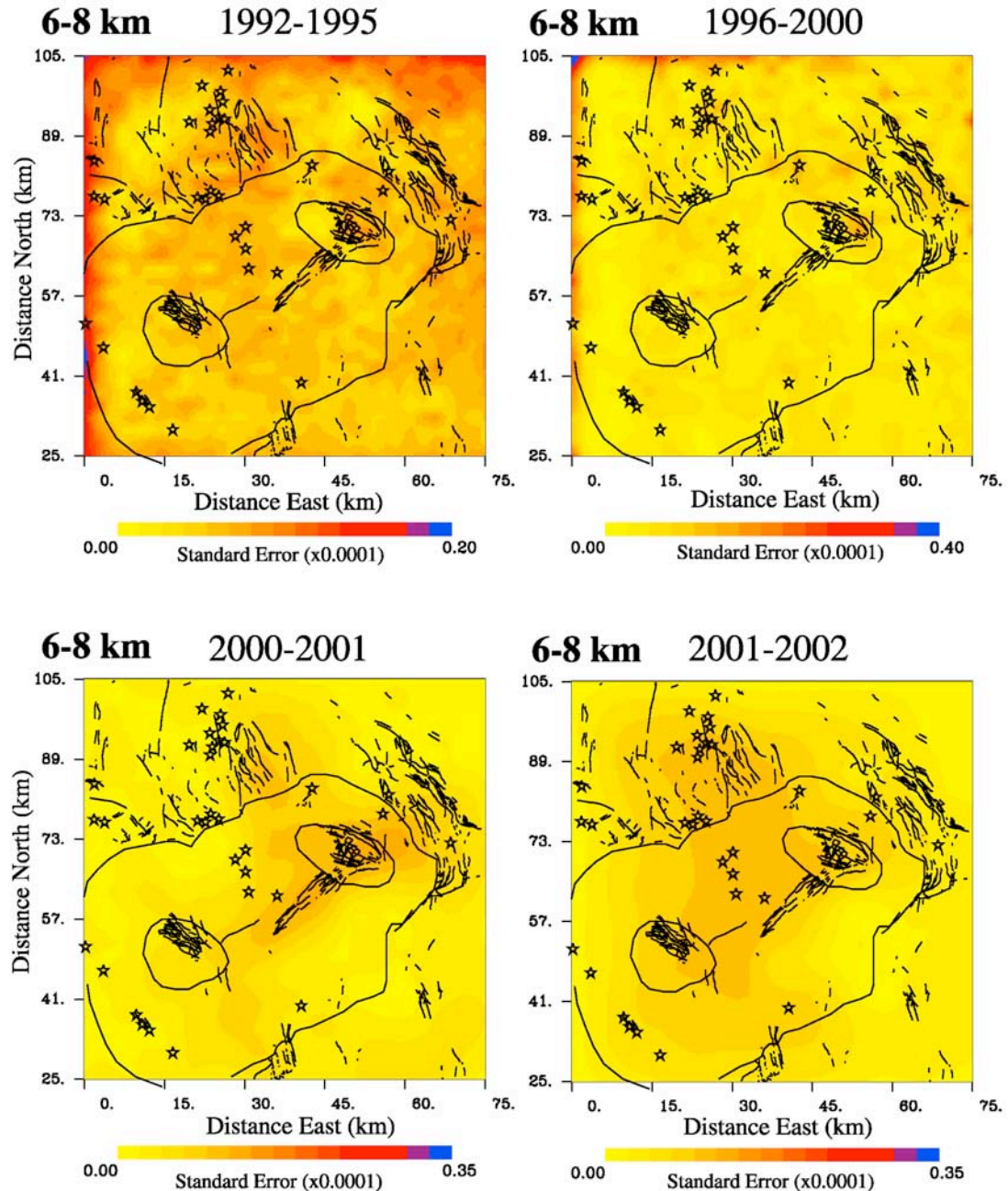


Figure 7. Error estimates associated with the volume changes in the uppermost layers containing volume decreases. The four models correspond to each of the four time intervals: 1992–1995, 1996–2000, 2000–2001, and 2001–2002. The estimates were obtained from 100 models generated by the inversion of the geodetic data which were contaminated by Gaussian noise. The variance of the noise was matched to the variance of the actual data.

3.2.2. 1996–2000

[31] In Figure 2, we plot the range change computed from the InSAR observations. Range decreases indicate that the surface of the Earth is moving closer to the observation

point in space. In many cases, the decrease in distance to the satellite is due to the uplift of the Earth's surface. The range change from 1996 to 2000 is dominated by a decrease at the northern edge of the caldera. This range decrease is sur-

Volume Increase Errors

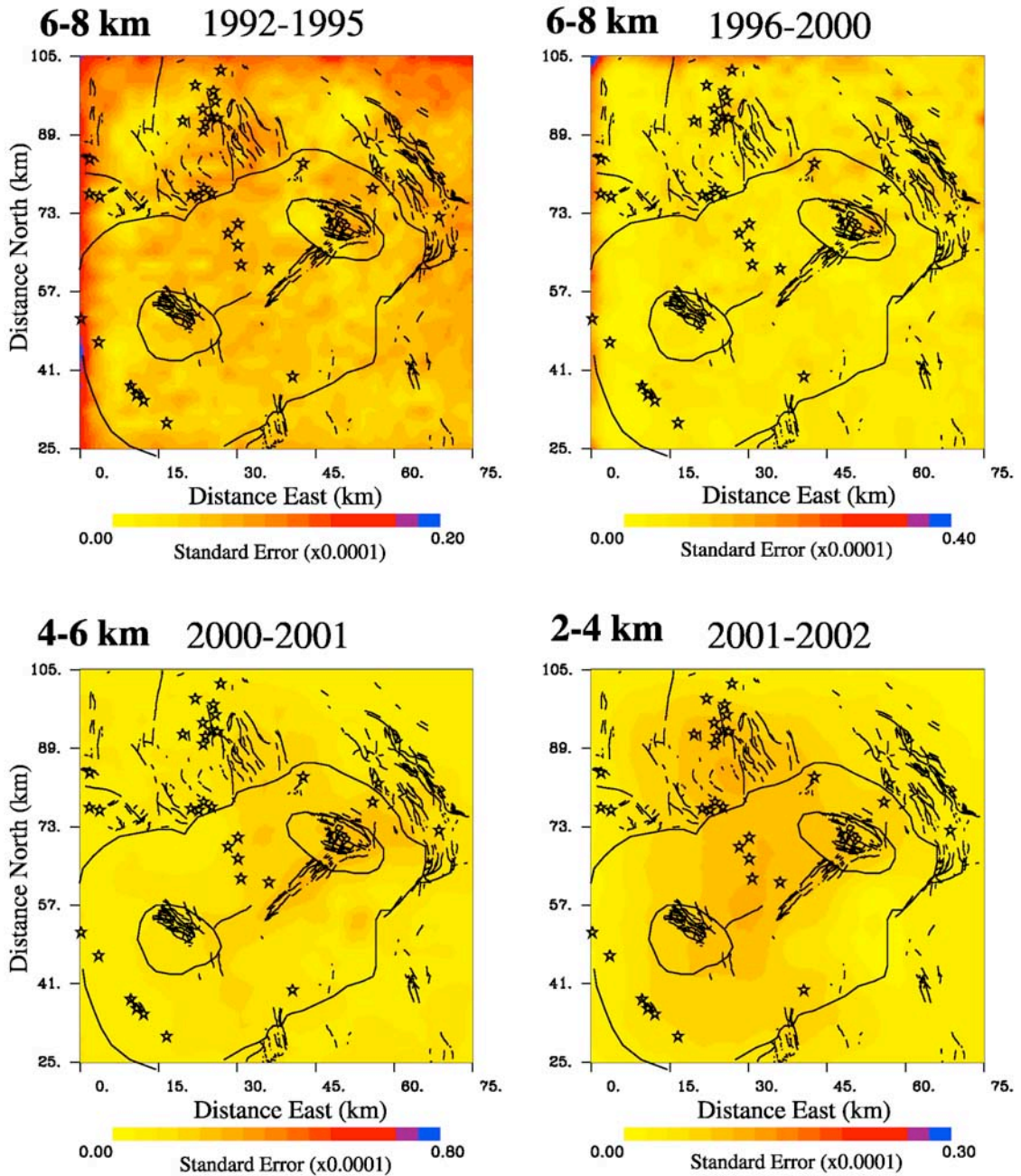


Figure 8. Error estimates associated with the volume increase in the uppermost layers of the models for each of the four time intervals: 1992–1995, 1996–2000, 2000–2001, and 2001–2002. The uppermost layer containing volume increases varies in depth for the different time intervals.

rounded by an intermittent ring of range increase, signifying subsidence. We have interpreted the pattern as evidence of an intrusion fed by a deeper source. In our modeling, we only estimate the volume increase associated with the intrusion. To this end, we incorporate positivity constraints into the inversion, only allowing for volume increases. The

additional constraints will help reduce the nonuniqueness associated with the inverse problem.

[32] The depth boundaries for this model are the same as for the previous model, 6–8 km for the uppermost layer. If we allow some degradation in the fit to the GPS data, it is possible to fit the observations with a significantly deeper

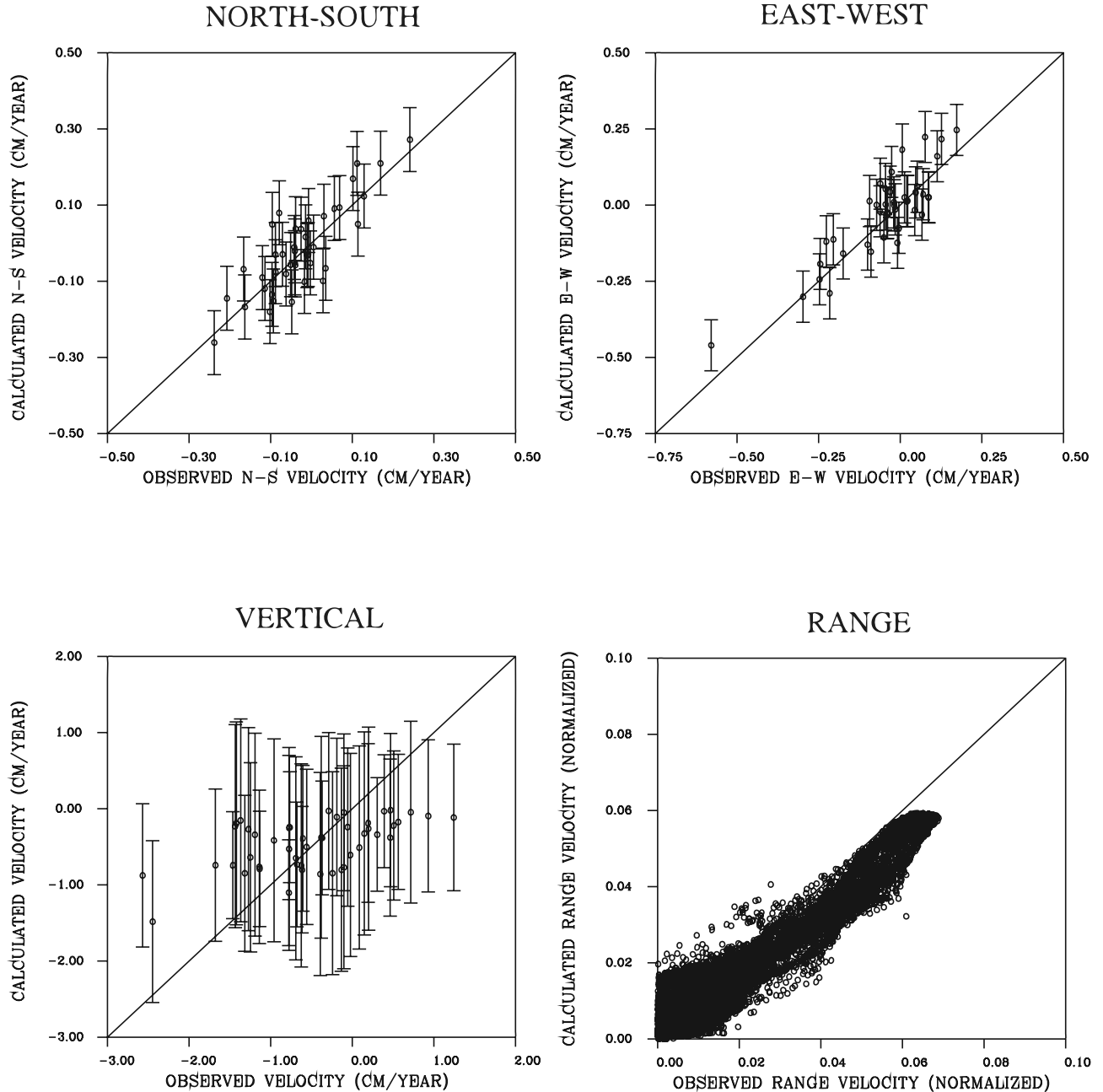


Figure 9. Observed GPS and InSAR range velocities plotted against velocities predicted using the fractional volume change model for the time interval 1992–1995. Error bars of one standard deviation are also plotted in the panels. For a perfect fit, the points would lie along the diagonal line in each figure.

source. That is, the InSAR observations can be fit by models which are below 10 km in depth. This fact illustrates the uncertainty associated with the depth estimates based upon surface deformation data.

[33] The subsurface volume change between 1996 and 2000 is dominated by an increase at the northern edge of the Yellowstone Caldera, just to the south of Norris Geyser Basin (Figure 6). The linear, north-trending volume increase in Figure 6 appears just to the west of the 1992–1995 volume decrease (Figure 5). The volume increase seems to be bounded on the north by the edge of the caldera, with the exception of a subtle north-trending feature which continues

toward the cluster of volcanic vents (Figure 6). Because of the positivity constraint, the volume decrease is uniformly zero (Figure 5). The volume change errors are shown in Figures 7 and 8. The noise level associated with the estimates is around $0.15\text{--}0.20 \times 10^{-4}$. This is roughly half of the peak anomaly in Figure 6, which is slightly less than 0.4×10^{-4} .

[34] The fit to the GPS data displays considerable scatter, and the error bars are of the order of 0.4 cm/year (Figure 10). The GPS data are generally fit to within their estimated uncertainties. Overall, the fit to the InSAR observations is quite good (Figure 10). Only the range decreases were fit, in

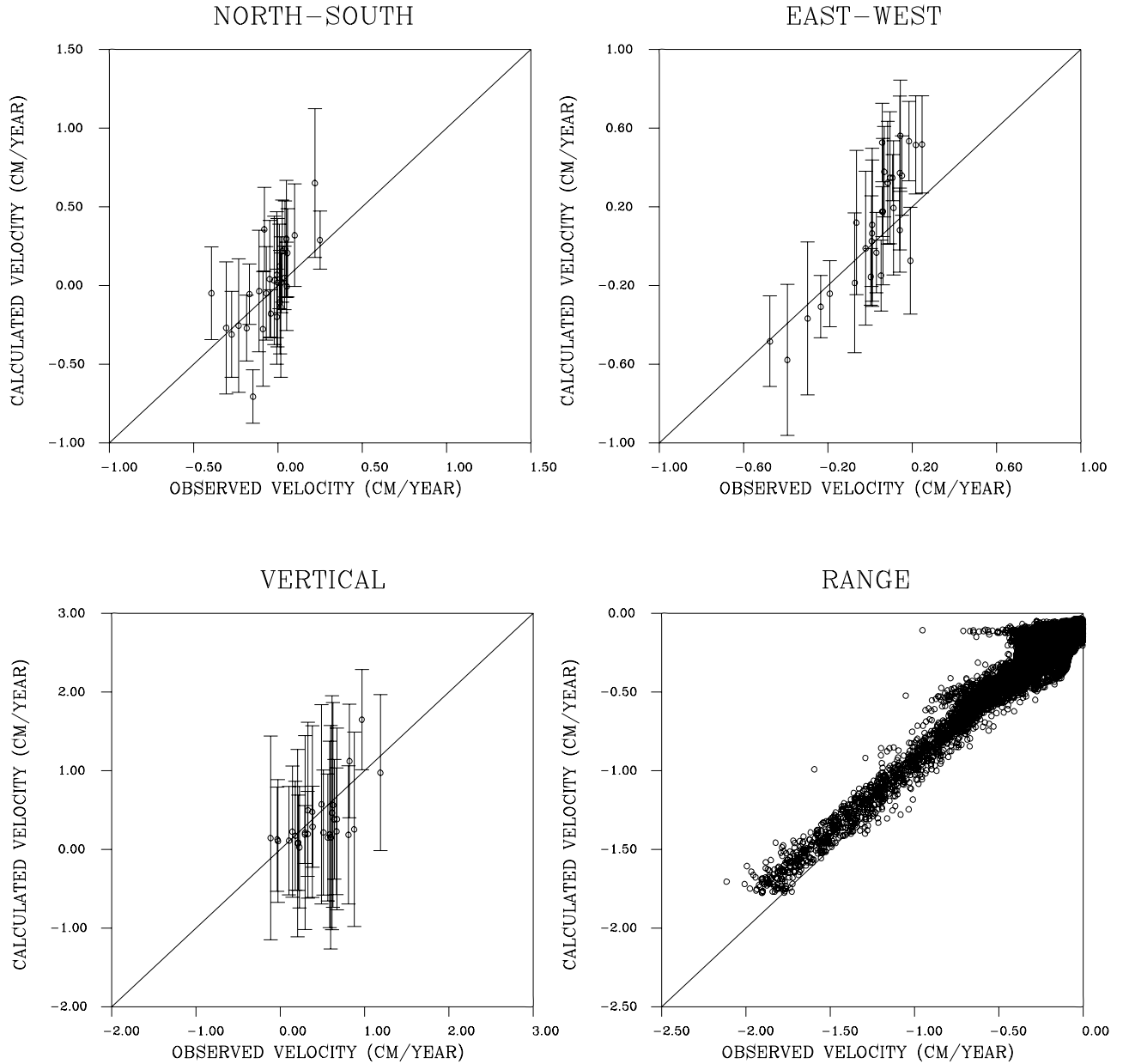


Figure 10. Observed GPS and InSAR range velocities plotted against velocities predicted using the fractional volume change model for the time interval 1996–2000. Error bars of one standard deviation are also plotted in the panels. For a perfect fit, the points would lie along the diagonal line in each figure.

keeping with the positivity constraint. The differences in the fits to the data may be due to the relative weighting of the GPS and InSAR data constraints.

3.2.3. 2000–2001

[35] Between the years 2000 and 2001, the range-change observations require a shallower volume change model, with layer boundaries of 4–6 and 6–8 km. For this time interval, we required volume increase in the uppermost layer (4–6 km) and volume decrease in the depth range 6–8 km. This distribution was intended to model a shallowing intrusion 4–6 km in depth and a continuing volume decrease within the semisolid magmatic body at 6–8 km. Such a distribution is nonunique and was chosen to be consistent with our modeling of the earlier time intervals.

[36] The pattern of volume change in the uppermost layer is composed of continued volume increases to the north (Figure 6). The volume increase is now concentrated along the caldera boundary. In the deeper layer, the volume decrease follows the north-east trending Elephant Back fault zone (Figure 5). The pattern is somewhat similar to the fractional volume decreases which occurred between 1992 and 1995. The errors associated with the estimates are shown in Figures 7 and 8. Both the volume decreases (Figure 5) and the volume increases (Figure 6) appear to exceed the estimated errors.

[37] The fit to the InSAR observations is shown in Figure 11. There is considerable scatter in the data, with up to a cm/year or more variation in the velocities. This is

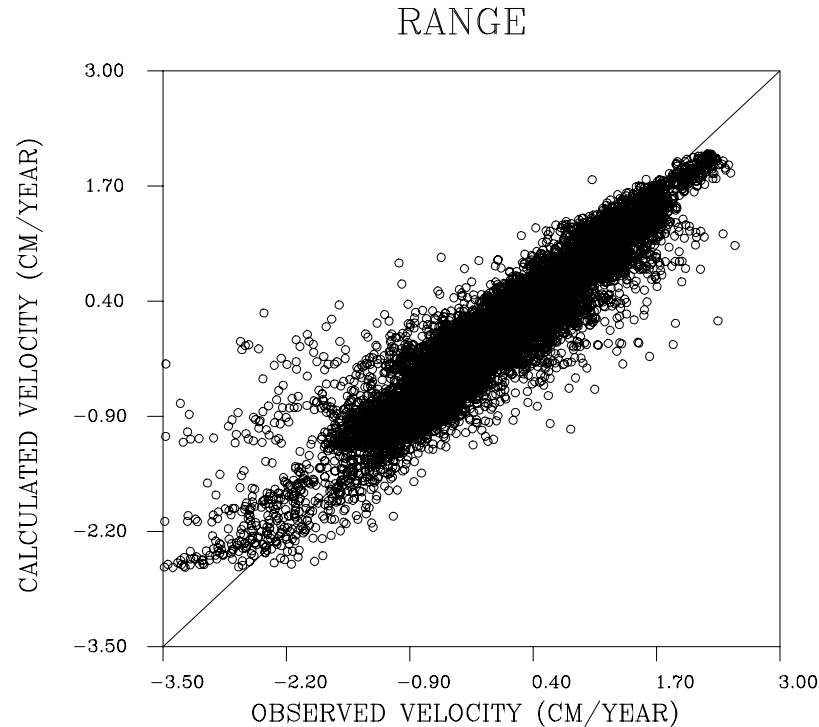


Figure 11. Observed InSAR range velocities for the period 2000–2001, plotted against range velocities predicted by the fractional volume change model.

likely due to the fact that the time interval is rather brief, this pair of images is only 1 year apart. The range-change estimates (Figure 2) contain considerable amplitude outside the caldera, in contrast to the earlier interferograms from 1992–1995 and 1996–2000. The shorter time intervals have accumulated less total deformation relative to the meteorological component. Still, the range change is fit relatively well, and the scatter does not exceed the estimated error level of 1 cm.

3.2.4. 2001–2002

[38] This time interval is also only a single year in duration and did not encompass GPS observations. Furthermore, the deformation due to the dynamics of the volcanic system seems reduced in amplitude, relative to the earlier time intervals. Consequently, the accumulated deformation is only moderately greater than the meteorological variations [Wicks *et al.*, 2006]. In fitting the InSAR data, we were required to include volume change in the depth range of 2 to 4 km. In addition, from Figure 2, it appears that subsidence is still occurring along the Elephant Back fault zone. In light of these two facts, we fixed the layer boundaries for this model at 2–4 and 6–8 km. The lower layer, 6–8 km in depth, is intended to model the semisolid magmatic body underlying the caldera. The volume changes in the shallow (2–4 km) layer are required to be positive, while deeper changes (6–8 km) are constrained to be negative. For the uppermost layer, the volume increases during this time period are concentrated along north-trending faults extending from the edge of the caldera (Figure 6). Only minor volume decreases are required at 6–8 km in depth in order to match the InSAR data (Figure 5). Slight volume decrease is found below the Sour Creek dome and along the eastern edge of the Elephant Back fault zone. However, these

volume changes are similar in magnitude to the changes outside the caldera. Where we consider the errors associated with the estimates (Figure 7), we find that the deeper volume decreases are not significant. However, the volume increases between 2 and 4 km do appear to exceed their estimated errors by a factor of two or more (Figure 8).

[39] The fit to the InSAR observations contains considerable scatter (Figure 12), as did the earlier 1-year interval (2000–2001). This is most likely due to meteorological variations. The peak scatter is of the order of 1 cm/year, roughly the size of the meteorological signal. Generally, most observations are fit to within 0.5 cm/year.

4. Discussion and Conclusions

[40] Based upon contemporary Yellowstone deformation, we find that subsurface volume changes correlate with the resurgent domes and the Elephant Back fault zone, north-trending extensional faults related to a line of volcanic vents, and the extensive magma body beneath the caldera. These correlations suggest that such features control or at least influence deformation within the caldera, either as zones of mechanical weakness or as pathways for fluid flow or both. There is evidence to support the role of both the Elephant Back fault zone and north-trending fault zones in both deformation, including fault slip, and fluid flow. The faults associated with the resurgent domes and the northeast-trending faults along the top of Elephant Back Mountain are some of the youngest normal faults in the caldera and offset glacial and alluvial material [Smith and Braile, 1994]. Furthermore, contemporary seismicity supports the notion that the volcanic vents southeast of Norris Geyser Basin are related to an active fault system that may continue southeasterly beneath the central caldera [Smith

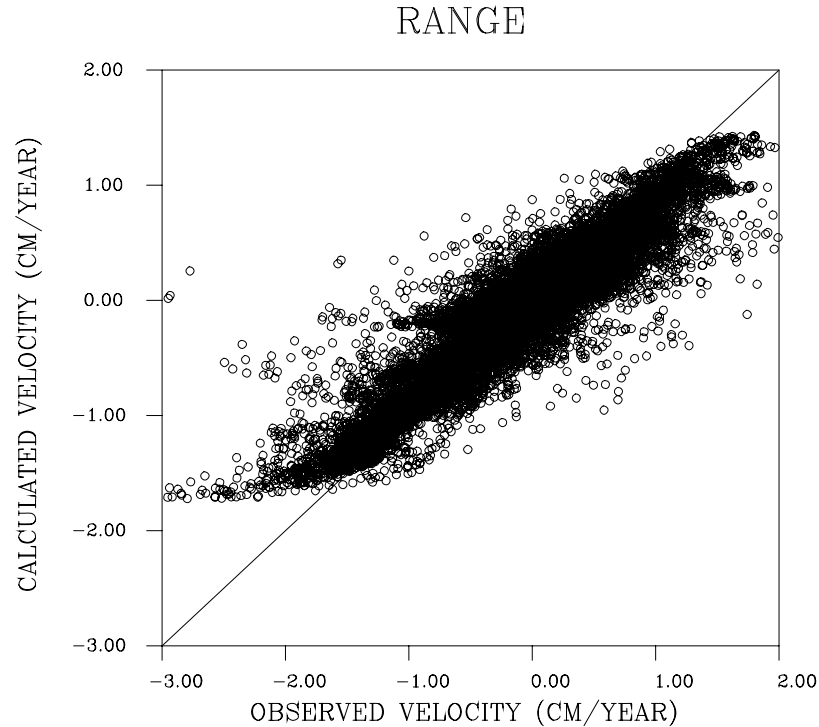


Figure 12. Observed InSAR range velocities for the period 2001–2002, plotted against range velocities predicted by the fractional volume change model.

and Braile, 1994; Waite and Smith, 2004; Husen et al., 2004]. The eastern edge of the first of the three superimposed calderas (caldera I) roughly coincides with this fault system and the line of volcanic vents [Smith and Braile, 1994]. There is evidence that a change from uplift to subsidence was preceded by an earthquake swarm along a fault intersecting the caldera [Waite and Smith, 2002]. Furthermore, the isotopic signature of CO_2 issuing from the intersection of the Elephant Back fault system [Pitt and Hutchinson, 1982] and in high flux sites [Werner et al., 2000] suggest a deep origin, evidence of a permeable pathway to the surface.

[41] We thus hypothesize that the observed surface deformation within and adjacent to the Yellowstone Caldera is due to the interaction of an underlying, large-scale crystallizing magmatic system and zones of weakness associated with crustal faults. In particular, large-scale pressure and mass changes within the magma body are focused into faults that act as narrow conduits or pathways for flow. The focused flow and pressure changes give rise to observable surface deformation. There are several lines of evidence supporting this hypothesis. First, as noted above, there is a clear association between subsurface volume changes and known or suspected faults within the caldera. The fact that the Elephant Back faults offset glacial and alluvial material indicates that this source of deformation is currently active. Second, the rapid and localized subsurface volume changes, such as the intrusion between 1996 and 2000, point to a relatively fast redistribution of mass at depth. Third, the linear trend of volcanic vents in the central portion of the caldera and to the north of the caldera, along the extension of the East Gallatin-Reese Creek fault zone, indicates that material has migrated up this zone of weakness. Fourth, tomographic imaging has revealed a well-defined low V_p

and positive V_p/V_s anomalies at the northern edge of the caldera, around 2 km deep, thought to represent a gas accumulation associated with the large magmatic body underlying the caldera [Husen et al., 2004]. This observation is evidence that material from the underlying magma body may indeed migrate to shallower depths. Fifth, helium isotopic ratios within the caldera suggest a deep origin [Kennedy et al., 1985], as does CO_2 near faults and thermal areas [Werner et al., 2000], supporting the idea that material does migrate to shallow depths.

[42] In Figure 13, we plot the three-dimensional configuration of the low P velocity anomaly, determined by earthquake tomography [Husen et al., 2004]. The low-velocity body underlies the two resurgent domes and the Elephant back fault zone, extending down to over 16 km in depth. In the figure, we also plot the volume decrease obtained by inverting the InSAR and GPS data (shown in map view in Figure 5). The volume decrease lies at the top of the low P velocity zone and follows the trend of the anomaly underlying the Elephant Back Fault zone. This correlation supports the idea that the volume change may be due to the dynamics of magmatic material underlying the brittle-plastic transition zone and fluid transported along faults. In Figure 14, we plot the volume increase obtained by inverting the 1996–2000 InSAR and GPS data. The volume increase lies at the same depth as the top of the inferred Yellowstone magma chamber interpreted from the low-velocity anomaly but is offset to the north and west. Such an offset suggests that the volume change may be independent of the dynamics of the intermediate depth magma body. There is a north-south trending component at the base of the low-velocity body which parallels and underlies the volume decrease. The correlation between

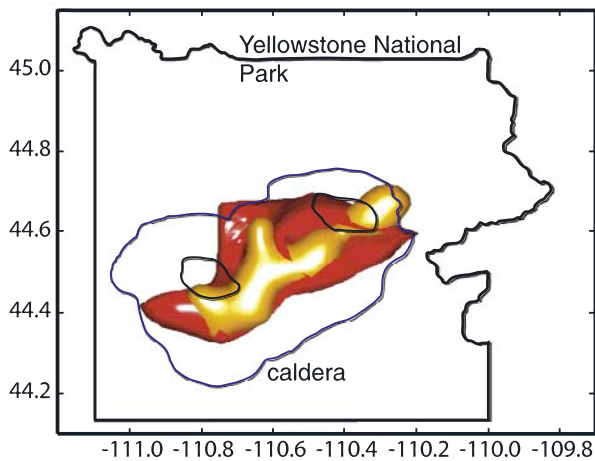
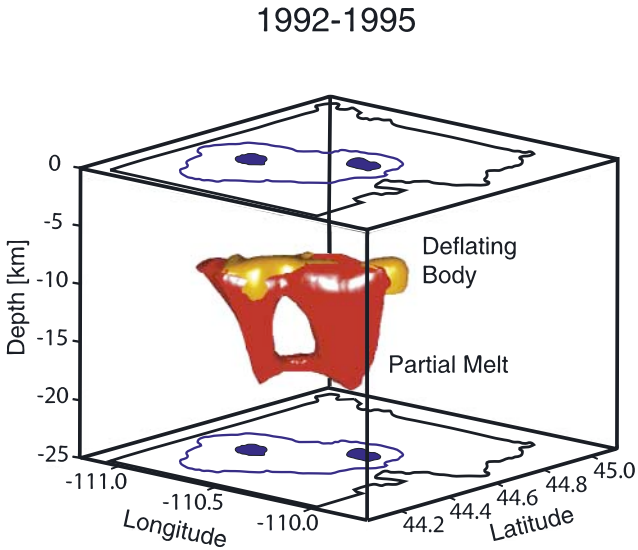


Figure 13. Three-dimensional rendering of the volume decrease from 1992 to 1995 (yellow) plotted over the low-velocity body imaged using seismic P wave tomography (red) [Husen *et al.*, 2004]. (a) The view obtained when looking from the southeast. (b) The volume decrease and seismic low velocity zone viewed from above.

these two structures is interesting and may reflect the importance of regional faults in the movement of magmatic fluids at depth.

[43] The association in space and time of volume decreases and increases at depth suggest a complicated physical system involving multiple components. A deep source, over 10 km below the surface, may represent the location of ponded basalts which either migrate or generate silicate melts. There is a shallower semisolid body at a depth of 5 km or deeper into which the magmatic material intrudes, perhaps a rhyolitic partial melt [Fournier, 1999]. The magmatic system is thought to be overlain by a self-sealing impermeable layer which acts to trap fluids and gases which are exsolved from the magma [Fournier, 1999]. The hydrothermal system, which lies above the self-sealing layer, transports fluids, gases, and heat to the surface [Dzurisin *et al.*, 1994]. Faults promote interaction between the various components of the system, mainly by providing permeable pathways for the

migration of gases from the magmatic to the hydrothermal component. The enhanced fluid movement may act to preferentially cool the magmatic body beneath the faults, further enhancing subsidence. The faults may also concentrate stress and promote intrusion and displacement along nearby faults. For example, between 2001 and 2002, a shallow (2–4 km) volume increase underlies faults to the north of the caldera. This volume change may be due to either actual fluid volume changes or due to extension along the faults induced by changes in the localized stress field within and/or around the caldera.

[44] We envision that the Yellowstone volcanic system involves the interaction of at least three subsystems: the shallow crustal hydrothermal system and seismogenic faults, the semisolid magmatic body, and a deeper underlying basaltic magma system. As yet, we cannot specify the exact nature of the interaction between these major components, and we can only draw very general conclusions about

1996-2000

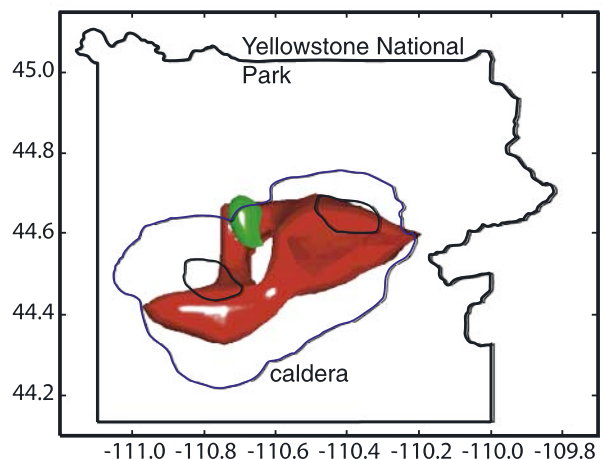
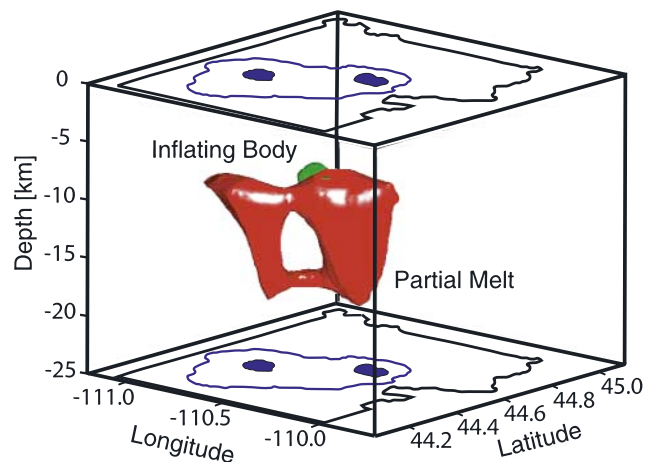


Figure 14. Three-dimensional rendering of the volume increase from 1996 to 2000 (green) plotted over the low-velocity body imaged using seismic P wave tomography (red) [Husen *et al.*, 2004]. (a) The view obtained when looking from the southeast. (b) The volume decrease and seismic low velocity zone viewed from above.

the influence of one component upon another. Specifically, the results here imply that crustal faults act as conduits for flow from within the Earth. Thus we are not proposing an encompassing model of the Yellowstone system, as given recently by *Wicks et al.* [2006].

[45] Continued observations, such as temporal changes in gravity, are necessary to differentiate between the detailed movements in the subsurface. Moreover, better constraints and more detailed sampling by the expanded University of Utah and EarthScope GPS arrays and more frequent acquisition of InSAR images will help unravel the sources of surface deformation at the Yellowstone Caldera. In particular, using descending and ascending InSAR data jointly, along with data InSAR reflecting at different look angles, will provide multiple components which will improve the modeling and inversion. Dense and continuous sampling in time will also help in following intrusive events and the migration of fluids.

[46] In the modeling, we have assumed that the volume changes are occurring in a homogeneous elastic Earth. However, due to thermal variations, there may be significant deviations from this assumption, particularly in depth. For example, it has been noted that a viscoelastic model can explain deformation at Long Valley caldera with a far more modest pressure change than a purely elastic model [*Newman et al.*, 2006].

[47] Though we have presented a spatially detailed model of subsurface volume change, there are several aspects of the modeling that can be improved. One enhancement would be to include the spatial variations in the computation of the Green's function, perhaps allowing for a depth-varying visco-elastic medium. We hope to include such variations in medium properties in a future study. In addition, on the basis of the results of this work, we could attempt to parameterize the volume change in a different fashion. That is, we could restrict the volume change to occur within the fault and fracture zones we have inferred in this study. This would reduce the nonuniqueness associated with the inverse problem and reduce the size of the inverse problem. In order to construct such a model, it will be necessary to include all important sources of volume change in the Yellowstone region, including the active magma bodies and important fractures and faults.

[48] **Acknowledgments.** We would like to thank Charles Wicks and Wayne Thatcher of the US Geological Survey for providing the InSAR estimates of range change used in this paper. The modeling work was supported by the Assistant Secretary, Office of Basic Energy Sciences of the US Department of Energy under contract DE-AC03-76SF00098. It was also supported by Assistant Secretary, Office of Geothermal Energy of the US Department of Energy under contract DE-AC03-76SF00098. We would also like to thank the National Science Foundation, Continental Dynamics and Earth Science program, for their support through grants EAR0314298, EAR9725431, EAR9316289, and EAR0225495, to the University of Utah for the GPS data acquisition, and to the NSF GEON project. The National Park Service provided permits to conduct the GPS surveys. Discussions on interpretations with Robert Fournier and Henry Heasler were particularly useful. All computations were carried out at the Center for Computational Seismology, Berkeley Laboratory.

References

- Aki, K., and P. G. Richards (1980), *Quantitative Seismology*, W. H. Freeman and Sons, San Francisco.
- Battaglia, M., and P. Segall (2004), The interpretation of gravity changes and crustal deformation in active volcanic areas, *Pure Appl. Geophys.*, *161*, 1453–1467.
- Bürgmann, R., P. A. Rosen, and E. J. Fielding (2000), Synthetic aperture radar interferometry to measure Earth's surface topography and its deformation, *Annu. Rev. Earth Planet. Sci.*, *28*, 169–209.
- Byrd, J. O. D., R. B. Smith, and J. W. Geissman (1994), The Teton Fault, Wyoming: Topographic signature, neotectonics, and mechanisms of deformation, *J. Geophys. Res.*, *99*, 20,095–20,122.
- Chang, W. L., and R. B. Smith (2002), Integrated earthquake hazard analysis of the Wasatch Front, Utah, *Bull. Seismol. Soc. Am.*, *92*, 1904–1922.
- Chinnery, M. A., and D. B. Jovanovich (1972), Effect of Earth layering on earthquake displacement fields, *Bull. Seismol. Soc. Am.*, *62*, 1629–1639.
- Dieterich, J. H., and R. W. Decker (1975), Finite element modeling of surface deformation associated with volcanism, *J. Geophys. Res.*, *80*, 4094–4102.
- Dzurisin, D., and K. M. Yamashita (1987), Vertical surface displacements at Yellowstone Caldera, Wyoming, 1976–1986, *J. Geophys. Res.*, *92*, 13,753–13,766.
- Dzurisin, D., J. C. Savage, and R. O. Fournier (1990), Recent crustal subsidence at Yellowstone Caldera, Wyoming, *Bull. Volcanol.*, *52*, 247–270.
- Dzurisin, D., K. M. Yamashita, and J. W. Kleinman (1994), Mechanisms of crustal uplift and subsidence at the Yellowstone Caldera, Wyoming, *Bull. Volcanol.*, *56*, 261–270.
- Dzurisin, D., C. Wicks, and W. Thatcher (1999), Renewed uplift at the Yellowstone Caldera measured by leveling surveys and satellite radar interferometry, *Bull. Volcanol.*, *61*, 349–355.
- Fournier, R. O. (1999), Hydrothermal processes related to movement of fluid from plastic into brittle rock in the magmatic–epithermal environment, *Econ. Geol.*, *94*, 1193–1211.
- Gabriel, A. K., R. M. Goldstein, and H. A. Zebker (1989), Mapping small elevation changes over large areas: Differential radar interferometry, *J. Geophys. Res.*, *94*, 9183–9191.
- Hestenes, M. R. (1980), *Conjugate Direction Methods in Optimization*, Springer, New York.
- Hoffmann, J., D. L. Galloway, and H. A. Zebker (2003), Inverse modeling of interbed storage parameters using land subsidence observations, Antelope Valley, California, *Water Resour. Res.*, *39*(2), 1031, doi:10.1029/2001WR001252.
- Husen, S., and R. B. Smith (2004), Probabilistic earthquake relocation in three-dimensional velocity models for the Yellowstone National Park region, Wyoming, *Bull. Seismol. Soc. Am.*, *94*, 880–896.
- Husen, S., R. B. Smith, and G. P. White (2004), Evidence for gas and magmatic sources beneath the Yellowstone Volcanic Field from seismic tomographic imaging, *J. Volcanol. Geotherm. Res.*, *131*(3–4), 397–410.
- Kennedy, B. M., M. A. Lynch, J. H. Reynolds, and S. P. Smith (1985), Intensive sampling of noble gases in fluids at Yellowstone: I. Early overview of the data; regional patterns, *Geochim. Cosmochim. Acta*, *49*, 1251–1261.
- Lawson, C. L., and R. J. Hanson (1974), *Solving Least Squares Problems*, Prentice-Hall, Upper Saddle River, N. J.
- Locke, W. W., and G. A. Meyer (1994), A 12,000-year record of vertical deformation across the Yellowstone Caldera margin: The shorelines of Yellowstone Lake, *J. Geophys. Res.*, *99*, 20,079–20,094.
- Maruyama, T. (1964), Static elastic dislocations in an infinite and semi-infinite medium, *Bull. Earthquake Res. Inst., Univ. Tokyo*, *42*, 289–368.
- Massonnet, D., and K. L. Feigl (1998), Radar interferometry and its application to changes in the Earth's surface, *Rev. Geophys.*, *36*, 441–500.
- Meertens, C. M., and R. B. Smith (1991), Crustal deformation of the Yellowstone Caldera from first GPS measurements: 1987–1989, *Geophys. Res. Lett.*, *18*, 1763–1766.
- Meertens, C. M., R. B. Smith, and C. M. Puskas (2000), Crustal deformation of the Yellowstone Caldera from campaign and continuous GPS surveys, 1987–2000, *Eos Trans. AGU*, *81*, 48.
- Newman, A. V., T. H. Dixon, G. Ofogobu, and J. E. Dixon (2001), Geodetic and seismic constraints on recent activity at Long Valley caldera, California: Evidence for viscoelastic rheology, *J. Volcanol. Geotherm. Res.*, *105*, 183–205.
- Newman, A. V., T. H. Dixon, and N. Gourmelen (2006), A four-dimensional viscoelastic deformation model for Long Valley Caldera, California, between 1995 and 2000, *J. Volcanol. Geotherm. Res.*, *150*, 244–269.
- Okada, Y. (1985), Surface deformation due to shear and tensile faults in a half space, *Bull. Seismol. Soc. Am.*, *75*, 1135–1154.
- Parker, R. L. (1975), The theory of ideal bodies for gravity interpretation, *Geophys. J. R. Astron. Soc.*, *42*, 315–334.
- Pelton, J. R., and R. B. Smith (1979), Recent crustal uplift in Yellowstone National Park, *Science*, *206*, 1179–1182.
- Pelton, J. R., and R. B. Smith (1982), Contemporary vertical surface displacements in Yellowstone National Park, *J. Geophys. Res.*, *87*, 2745–2761.

- Pitt, A. M., and R. A. Hutchinson (1982), Hydrothermal changes related to earthquake activity at Mud Volcano, Yellowstone National Park, Wyoming, *J. Geophys. Res.*, *87*, 2762–2766.
- Puskas, C. M., R. B. Smith, and C. M. Meertens (1998), Crustal deformation of the Yellowstone Plateau from GPS and seismicity, *Eos Trans. AGU*, *79*(45), F949.
- Puskas, C., R. B. Smith, C. M. Meertens, and W. L. Chang (2007), Crustal deformation of the Yellowstone-Snake River Plain volcano-tectonic system: Campaign and continuous GPS observations, 1987–2004, *J. Geophys. Res.*, *112*, B03401, doi:10.1029/2006JB004325.
- Reilinger, R. E., G. P. Citron, and L. D. Brown (1977), Recent vertical crustal movements from precise leveling data in southwestern Montana, western Yellowstone National Park, and the Snake River Plain, *J. Geophys. Res.*, *82*, 5349–5359.
- Roach, G. F. (1970), *Green's Functions: Introductory Theory with Applications*, Van Nostrand Reinhold, Hoboken, N. J.
- Sabatier, P. C. (1977), Positivity constraints in linear inverse problems-I. General theory, *Geophys. J. R. Astron. Soc.*, *48*, 415–441.
- Savage, J. C., M. Lisowski, W. H. Prescott, and A. M. Pitt (1993), Deformation from 1973 to 1987 in the epicentral area of the 1959 Hebgen Lake, Montana, earthquake ($M_s = 7.5$), *J. Geophys. Res.*, *98*, 2145–2153.
- Smith, R. B., and L. W. Braile (1994), The Yellowstone hotspot, *J. Volcanol. Geotherm. Res.*, *61*, 121–187.
- Smith, R. B., and C. Meertens (1989), Network analysis and inter-campaign comparison of GPS results from the 1987 Yellowstone-Hebgen Lake-Teton crustal deformation experiment, *Eos Trans. AGU*, *70*, 309.
- Stakgold, I. (1979), *Green's Function and Boundary Value Problems*, John Wiley, Hoboken, N. J.
- Strange, W. E. (1981), The impact of refraction corrections on leveling interpretations in southern California, *J. Geophys. Res.*, *86*, 2809–2824.
- Vasco, D. W., and L. R. Johnson (1985), Extremal inversion of static earth displacements due to volume sources, *Geophys. J. R. Astron. Soc.*, *80*, 223–239.
- Vasco, D. W., L. R. Johnson, and N. E. Goldstein (1988), Using surface displacement and strain observations to determine deformation at depth, with an application to Long Valley Caldera, California, *J. Geophys. Res.*, *93*, 3232–3242.
- Vasco, D. W., R. B. Smith, and C. L. Taylor (1990), Inversion for sources of crustal deformation and gravity change at the Yellowstone Caldera, *J. Geophys. Res.*, *95*, 19,839–19,856.
- Vasco, D. W., C. Wicks, K. Karasaki, and O. Marques (2002a), Geodetic imaging: Reservoir monitoring using satellite interferometry, *Geophys. J. Int.*, *149*, 555–571.
- Vasco, D. W., K. Karasaki, and O. Nakagome (2002b), Monitoring production using surface deformation: The Hijiori test site and the Okuaizu geothermal field, Japan, *Geothermics*, *31*, 303–342.
- Waite, G. P., and R. B. Smith (2002), Seismic evidence for fluid migration accompanying subsidence of the Yellowstone Caldera, *J. Geophys. Res.*, *107*(B9), 2177, doi:10.1029/2001JB000586.
- Waite, G. P., and R. B. Smith (2004), Seismotectonics and stress field of the Yellowstone volcanic plateau from earthquake first-motions and other indicators, *J. Geophys. Res.*, *109*, B02301, doi:10.1029/2003JB002675.
- Werner, C., S. L. Brantley, and K. Boomer (2000), CO₂ emissions related to the Yellowstone volcanic system 2. Statistical sampling, total degassing, and transport mechanisms, *J. Geophys. Res.*, *105*, 10,831–10,846.
- Wicks, C., W. Thatcher, and D. Dzurisin (1998), Migration of fluids beneath Yellowstone Caldera inferred from satellite radar interferometry, *Science*, *282*, 458–462.
- Wicks, C. W., W. Thatcher, D. Dzurisin, and J. Svare (2006), Uplift, thermal unrest, and magma intrusion at Yellowstone Caldera, *Nature*, *440*, 72–75.
- Zebker, H. A., P. A. Rosen, R. M. Goldstein, A. Gabriel, and C. L. Werner (1994), On the derivation of coseismic displacement fields using differential radar interferometry: The Landers earthquake, *J. Geophys. Res.*, *99*, 19,617–19,634.

C. M. Meertens, UNAVCO, 6350 Nautilus Drive, Boulder, CO 80301-5554, USA.

C. M. Puskas and R. B. Smith, Department of Geology and Geophysics, University of Utah, Salt Lake City, UT 84112, USA.

D. W. Vasco, Berkeley Laboratory, University of California, Berkeley, CA, USA. (dwvasco@lbl.gov)